BAMS Article

Tara Pacific Expedition's Atmospheric Measurements of Marine Aerosols across the Atlantic and Pacific Oceans

Overview and Preliminary Results

J. M. Flores, G. Bourdin, O. Altaratz, M. Trainic, N. Lang-Yona, E. Dzimban, S. Steinau, F. Tettich, S. Planes, D. Allemand, S. Agostini, B. Banaigs, E. Boissin, E. Boss, E. Douville, D. Forcioli, P. Furla, P. E. Galand, M. B. Sullivan, É. Gilson, F. Lombard, C. Moulin, S. Pesant, J. Poulain, S. Reynaud, S. Romac, S. Sunagawa, O. P. Thomas, R. Troublé, C. de Vargas, R. Vega Thurber, C. R. Voolstra, P. Wincker, D. Zoccola, C. Bowler, G. Gorsky, Y. Rudich, A. Vardi, and I. Koren

ABSTRACT: Marine aerosols play a significant role in the global radiative budget, in clouds' processes, and in the chemistry of the marine atmosphere. There is a critical need to better understand their production mechanisms, composition, chemical properties, and the contribution of ocean-derived biogenic matter to their mass and number concentration. Here we present an overview of a new dataset of in situ measurements of marine aerosols conducted over the 2.5-yr *Tara* Pacific Expedition over 110,000 km across the Atlantic and Pacific Oceans. Preliminary results are presented here to describe the new dataset that will be built using this novel set of measurements. It will characterize marine aerosols properties in detail and will open a new window to study the marine aerosol link to the water properties and environmental conditions.

https://doi.org/10.1175/BAMS-D-18-0224.1

Corresponding author: J. Michel Flores, flores@weizmann.ac.il; Ilan Koren, ilan.koren@weizmann.ac.il; and Assaf Vardi, assaf.vardi@weizmann.ac.il

In final form 10 December 2019

AFFILIATIONS: Flores, Altaratz, Trainic, Rudich, and Koren—Department of Earth and Planetary Sciences, Weizmann Institute of Science, Rehovot, Israel; **Bourdin**—School of Marine Sciences, University of Maine, Orono, Maine, and Sorbonne Université, CNRS, Laboratoire d'Océanographie de Villefranche, Villefranche-sur-Mer, France; **Lang-Yona* and Vardi**—Department of Plant and Environmental Science, Weizmann Institute of Science, Rehovot, Israel; **Dzimban, Steinau, and Tettich**—Grimm Aerosol Technik, Ainring, Germany; **Planes**—Laboratoire d'Excellence CORAIL, PSL Research University, EPHE-UPVD-CNRS, USR 3278 CRIOBE, Université de Perpignan, Perpignan, and Research Federation for the Study of Global Ocean Systems Ecology and Evolution, FR2022/*Tara* Oceans-GOSEE, Paris, France; **Allemand, Reynaud, and Zoccola**—Centre Scientifique de Monaco, Monaco; **Agostini**—Shimoda Marine Research Center, University of Tsukuba, Shizuoka, Japan; **Banaigs and Boissin**—Laboratoire d'Excellence CORAIL, PSL Research University, EPHE-UPVD-CNRS, USR 3278 CRIOBE, Université de Perpignan, Perpignan, France; **Boss**—School of Marine Sciences, University of Maine, Orono, Maine; **Douville**—Laboratoire des Sciences du Climat et de l'Environnement, LSCE/IPSL, CEA-CNRS-UVSQ, Université Paris-Saclay, Gif-sur-Yvette, France; **Forcioli and Furla**—Université Côte d'Azur, CNRS, INSERM, IRCAN, Medical School; **Gilson**—Université Côte d'Azur, CNRS, INSERM, IRCAN, Medical School, and Department of Medical Genetics, Centre Hospitalier Universitaire de Nice, Nice, France; **Galand**—Research Federation for the Study of Global Ocean Systems Ecology and Evolution, FR2022/*Tara* Oceans-GOSEE, Paris, and Sorbonne Université, CNRS, Laboratoire d'Ecogéochimie des Environnements Benthiques (LECOB), Observatoire Océanologique de Banyuls, Banyuls sur mer, France; **Sullivan**—Department of Microbiology, and Department of Civil, Environmental and Geodetic Engineering, and Byrd Polar and Climate Research Center, The Ohio State University, Columbus, Ohio; **Lombard**—Sorbonne Université, CNRS, Laboratoire d'Océanographie de Villefranche, F-06230 Villefranche-sur-Mer, France, and Institut Universitaire de France (IUF), Paris, France; **Gorsky**—Sorbonne Université, CNRS, Laboratoire d'Océanographie de Villefranche, F-06230 Villefranche-sur-Mer, France; **Moulin**—The *Tara* Ocean Foundation, Paris, France; **Pesant***—PANGEA, and Center for Marine Environmental Sciences, Universität Bremen, Bremen, Germany; **Poulain**—Research Federation for the Study of Global Ocean Systems Ecology and Evolution, FR2022/*Tara* Oceans-GOSEE, Paris, and Génomique Métabolique, Genoscope, Institut François Jacob, CEA, CNRS, Univ. Evry, Université ParisSaclay, Evry, France; **Romac**—Research Federation for the Study of Global Ocean Systems Ecology and Evolution, FR2022/*Tara* Oceans-GOSEE, Paris, and Sorbonne Université, CNRS, Station Biologique de Roscoff, AD2M, UMR 7144, ECOMAP, Roscoff, France; **Sunagawa**—Department of Biology and Swiss Institute of Bioinformatics, ETH Zürich, Zürich, Switzerland; **Thomas**—Marine Biodiscovery Laboratory, School of Chemistry and Ryan Institute, National University of Ireland, Galway, Galway, Ireland; **Troublé**—The *Tara* Ocean Foundation, Paris, France, and Research Federation for the Study of Global Ocean Systems Ecology and Evolution, FR2022/*Tara* Oceans-GOSEE; **de Vargas**—Research Federation for the Study of Global Ocean Systems Ecology and Evolution, FR2022/*Tara* Oceans-GOSEE, Paris, and Sorbonne Université, CNRS, Station Biologique de Roscoff, AD2M, UMR 7144, ECOMAP, Roscoff, France; **Vega Thurber**—Department of Microbiology, Oregon State University, Corvallis, Oregon; **Voolstra**—Department of Biology, University of Konstanz, Konstanz, Germany; **Wincker**—Research Federation for the Study of Global Ocean Systems Ecology and Evolution, FR2022/*Tara* Oceans-GOSEE, Paris, and Génomique Métabolique, Genoscope, Institut François Jacob, CEA, CNRS, Univ. Evry, Université Paris-Saclay, Evry, France; **Bowler**—Research Federation for the Study of Global Ocean Systems Ecology and Evolution, FR2022/*Tara* Oceans-GOSEE, and Institut de Biologie de l'Ecole Normale Supérieure, Ecole normale supérieure, CNRS, INSERM, Université PSL, Paris, France

*** CURRENT AFFILIATION: Lang-Yona**—Kinneret Limnological Laboratory, Israel Oceanographic and Limnological Research, Migdal, Israel; **Pesant**—European Molecular Biology Laboratory, European Bioinformatics Institute, Wellcome Genome Campus, Hinxton, Cambridge CB10 1SD, United Kingdom

Marine aerosol, defined here as the aerosol present in the marine atmospheric boundary layer, consists of natural and anthropogenic components. It originates over ocean or land (by a variety of production processes) and can be transported over large distances (Brooks and Thornton 2018). The main component (by mass) of marine aerosol, termed sea spray aerosol (SSA; De Leeuw et al. 2011; Boucher et al. 2013), is produced by primary processes through the mechanical interaction of wind with the ocean surface. Secondary marine aerosol can be produced from oxidation products of volatile organic compounds, the best known resulting from the oxidation of dimethylsulphide (Charlson et al. 1987), or chemical transformation of primary or secondary components present in the condensed phase (Rinaldi et al. 2010; Ramachandran 2018). There is still great uncertainty regarding SSA production fluxes and its dependence on oceanic (like water temperature, salinity, or the presence of organics) and atmospheric (e.g., relative humidity, atmospheric instability) conditions (De Leeuw et al. 2011; Lewis and Schwartz 2004; De Leeuw et al. 2011; Textor et al. 2006; Kinne et al. 2006). Current estimates of global SSA mass in the atmosphere range between 0.02 and 1×10^{14} kg yr^{-1} (Textor et al. 2006). There are also large uncertainties related to SSA radiative cooling effect, with estimates in the range of 0.08–6 W m^{-2} (Lewis and Schwartz 2004), and its contribution to total aerosol optical depth, ranging between 18% and 50% (De Leeuw et al. 2014). Unlike optical depth and mass concentration, estimates of the emitted SSA size distribution can be constrained only by in situ measurements (Heintzenberg et al. 2000; Jaeglé et al. 2011). SSA also plays a major role in aerosol–cloud interactions determining the initial size distribution and number concentration of drops in marine clouds (O'Dowd et al. 1999; Pierce and Adams 2006).

Transport of aerosols from the continents to the marine environment (including pollution, pollen, mineral dust, etc.) is also a major source of marine aerosol. Mineral dust is a predominate aerosol type over the continents, and since it can be transported for thousands of kilometers (Van der Does et al. 2018; Ben-Ami et al. 2012; Middleton et al. 2001; Betzer et al. 1988; Duce et al. 1980) it is a major component in marine aerosol as well. The characterization of mineral dust aerosol is of great importance, as it is currently a significant fraction of the particulate burden in the marine boundary layer, and with climate change expected trends (i.e., enhanced droughts and desertification), there can be a dramatic increase of mineral dust injected into the troposphere in general and also into the marine boundary layer (Woodward et al. 2005). Furthermore, its radiative forcing is still undefined, it can be positive (heating) or negative (cooling) (Boucher et al. 2013), and due to the lack of sufficient data its scattering properties are not easy to determine. Mineral dust aerosols can also serve as sources of primary productivity, they have been shown to provide particulate iron phosphate essential for bloom-forming in the oceans from continental sources (Martin et al. 1994). Additionally, while being transported, mineral dust can be processed in the air or within clouds, changing its chemical properties (Andreae et al. 1986).

Although significant progress has been achieved in our understanding of the role of marine aerosol in clouds' processes, radiation balance, and chemistry of the marine atmosphere, there are still large gaps in our knowledge that are considered as major sources of uncertainty in our capability to predict the climate (Boucher et al. 2013; Carslaw et al. 2017). Therefore, it is necessary to characterize marine aerosol particles, and understand their formation mechanisms and their physical and chemical changes as they are transported.

Marine aerosol measurements were collected during the *Tara* Pacific Expedition (Planes et al. 2019; Gorsky et al. 2019) along the approximately 110,000 km route in the Atlantic and Pacific Oceans (see the route in Fig. 1). Measurements were conducted in various oceanic and atmospheric conditions and at different distances from the continent. The primary research

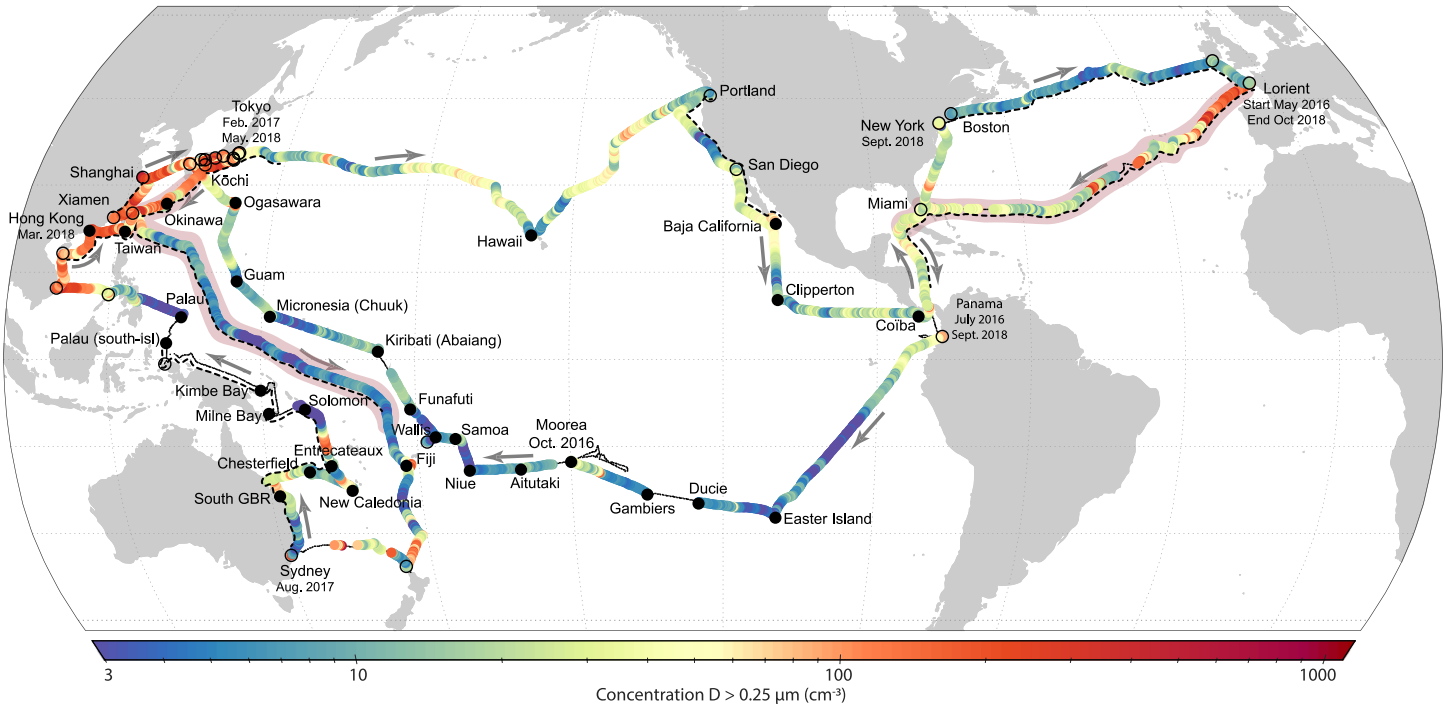

Fig. 1. Route of the *Tara* Pacific Expedition 2016–18 visualized by the OPC aerosol concentration of $D > 0.25$ µm. The black line shows the full route of the expedition, but where no aerosol data were collected. The gray arrows indicate the direction *Tara* sailed. The black dotted line shows the areas the SMPS was working. The black full circles denote coral holobionte sampling sites, and the black open circles denote any other stopover. The expedition was mainly dedicated to coral reefs providing us with a balance between cruising mode that covers large oceanic domains to detailed measurements at specific locations near islands in the open ocean and costal zones.

goals of the R/V *Tara*'s Pacific marine-atmosphere-measurements suite were 1) to characterize marine aerosol's physical, chemical, and biological properties across open ocean and coastal areas in the Atlantic and Pacific oceans and 2) to understand links and feedbacks between the ocean surface mixed layer and the atmospheric boundary layer properties. Here we describe the atmospheric measurements done in this unprecedented scientific campaign and present preliminary results that demonstrate the comprehensive database of marine aerosol's properties we are currently building.

Tara Pacific expedition 2016–18

In May 2016, the *Tara* Ocean Foundation (see Appendix E) embarked in its eleventh expedition, the *Tara* Pacific Expedition, a 2.5-yr research project aimed to understand coral reef holobiont and its associated surface plankton ecosystem (Planes et al. 2019), and to assess inter-island and open-ocean surface plankton community structures (Gorsky et al. 2019). The *Tara* Pacific Expedition mainly took place in the Pacific Ocean, and while performing the coral reef studies, surface ocean measurements together with detailed aerosol measurements were performed all along *Tara*'s route (Fig. 1).

The ocean surface measurements included continuous monitoring of inherent optical properties, sea surface salinity and temperature, and net community production. Additionally, daily, discrete sampling consisted of high-performance liquid chromatography, carbonate chemistry, and micro- and macronutrients but also taxonomic and genomic studies of plankton spanning from viruses to mesozooplankton. The details of the oceanic measurements can be found in Gorsky et al. (2019).

For the atmospheric measurements, we installed instrumentation for continuous online aerosol measurement (see details in the next section), wide-angle time-lapse cameras to record

the state of the ocean and the clouds, as well as a custom-made filters system for biological, chemical, and morphological analysis of the marine aerosols. The previous long-term expedition, *Tara* Oceans, focused on ocean measurements of the sub-superficial, deep chlorophyll and mesopelagic communities. The *Tara* Pacific Expedition, covering over 110,000 km, is the first time *Tara* includes marine aerosol measurements along with the surface ocean measurements. The parallel marine-atmosphere-measurements suite and the measurements of the surface of the ocean properties will allow us to establish a comprehensive database that will enable a better understanding of marine aerosol's properties and their link to ocean–atmosphere interaction and feedbacks.

R/V *Tara* and atmospheric instrumentation

Tara is a 36-m-long, 10-m-wide aluminum hull schooner with two 27-m masts (Fig. 2). *Tara* was equipped with a meteorological station [Station Bathos II Météo France, located ~7 m above mean sea level (MSL)] measuring air temperature, relative humidity, and pressure. The wind speed and direction were measured at the top of the mast, ~27 m MSL, and the water temperature and salinity were measured by a thermo-salinometer (Sea-Bird Electronics SBE45 MicroTSG). Its main water entrance was located in the hull, 1.5 m under the waterline, so depending on ocean conditions the water was sampled 0.5–3 m under the sea surface. The photosynthetically active radiation (solar radiation from 400 to 700 nm) was measured next to the weather station by a QCR-2150 (Biospherical Instruments Inc.), recorded continuously and averaged per minute. Daily measurements of atmospheric transmittance were performed using a five-channel Microtops II loaned from NASA (Smirnov et al. 2006) and a radiometer system (SIMBADA; Deschamps et al. 2004).

Fig. 2. R/V *Tara* instrument setup for the *Tara* Pacific Expedition. The inlet for aerosol sampling was installed along the backstay. For the first Atlantic crossing the inlet was installed halfway up the backstay. The main water entrance is located in the hull 1.5 m under the waterline; depending on ocean conditions the water will be sampled between 0.5 and 3 m under the sea surface. A detailed description of the surface water measurements can be read in Gorsky et al. (2019), and the coral reef measurements in Planes et al. (2019).

Three aerosol instruments were installed aboard *Tara*: 1) a scanning mobility particle sizer (SMPS, SMPS-C GRIMM Aerosol Technik Ainring GmbH and Co. KG, Ainring, Germany) for size distribution measurements from 0.01 to 1.089 μm; 2) an optical particle counter (OPC; EDM180 GRIMM Aerosol Technik Ainring GmbH and Co. KG, Ainring, Germany) for size distribution measurements from 0.25 to 32 μm; and 3) a custom-made aerosol filter system consisting of four 47-mm filter holders and one vacuum pump (Diaphragm pump ME 16 NT, VACUUBRAND BmbH and Co KG, Wertheim, Germany).

A Nafion dryer was installed before the SMPS and OPC, which reduced the sampled air relative humidity to below 40%. An extra diffusion dryer was installed between the Nafion and the SMPS to further dry the air before entering the SMPS.

Two separate inlets, located next to each other, one for the SMPS–OPC system and one for the filter system, were constructed out of conductive tubing of 1.9 cm inner diameter and a funnel (allowing the collection of all diameters) and mounted on the rear backstay of *Tara* (see appendix A for more details). The flow through the SMPS–OPC system was 1.5 L min^{-1} (lpm). The flow through the filter system was 80 lpm (20 lpm for each filter) during the first Atlantic crossing up to Miami, and 120 lpm (30 lpm for each filter) after this point. For the measurements from Lorient, France, to Miami, United States, the inlets were installed halfway up the backstay (~15 m MSL) and after Miami, the inlets were relocated to the top of the backstay (~27 m MSL). The SMPS was set to do a full scan of the particle distribution every 5 min and the OPC produced a particle size distribution every 60 s; both instruments were set to measure continuously throughout the expedition and were time-synchronized with the UTC date and time of *Tara*'s GPS. To have accurate marine aerosol size distributions and total concentrations, the SMPS–OPC data were corrected for particle loss (Von der Weiden et al. 2009) and engine contamination and were merged using the method described by Hand and Kreidenweis (2002) (see appendix A).

The filters from the custom-made system were changed, in general, twice a day, collecting aerosols for periods of at least 12 h. Three filter holders contained 0.45 μm PVDF membrane filters (HVLP04700, Durapore) that were folded into a 2-mL cryotube and immediately dropped into liquid nitrogen after each collection period. The fourth filter holder contained 0.8-μm polycarbonate filters (ATTP04700, Millipore) that were stored at room temperature in PetriSlide dishes preloaded with absorbent pads (Millipore, PDMA04700) to keep the filters dry while stored.

Results

Marine aerosol size distributions. To compare the Atlantic and Pacific Oceans' measurements in similar seasons, we analyzed two sailing periods: one of two months between April and May 2017 in the Pacific Ocean, and one of 35 days in May–June 2016 over the Atlantic. Figure 3 shows the total aerosol concentration and size distributions for the two sailing periods, on the left, the Japan–Taiwan–Fiji leg and, on the right, the Lorient–Miami leg with 48-h back trajectories (Rolph et al. 2017; Stein et al. 2015) shown in different colors. The presented trajectories are the average trajectories of the "ensemble option" that were calculated based on an endpoint at 250-m height, which is the minimum height for the optimal configuration of the ensemble.

In the western Pacific Ocean, two clear, distinct scenarios can be seen: the first is the Kochi, Okinawa, and Keelung stopovers, and the second is the open ocean sailing toward Fiji. In the open-ocean period, with eastern origin of the air masses, far from continental influence, there is an average total aerosol concentration of 180 (±51) cm^{-3}, with 83 (±30) cm^{-3} aerosol with diameters $D > 0.1$ μm which can be considered, in general, cloud condensation nuclei (CCN) for supersaturation ≥0.4% (Dusek et al. 2006). After a daylong rain period (13–14 May) the total aerosol concentration decreased to 82 cm^{-3} and to 13 cm^{-3} for $D > 0.1$ μm. Most of the transect is characterized by a bimodal distribution, but after the rainy period, we see a single Aitken-mode distribution with a mode diameter of around 0.031 μm. The aerosol concentration

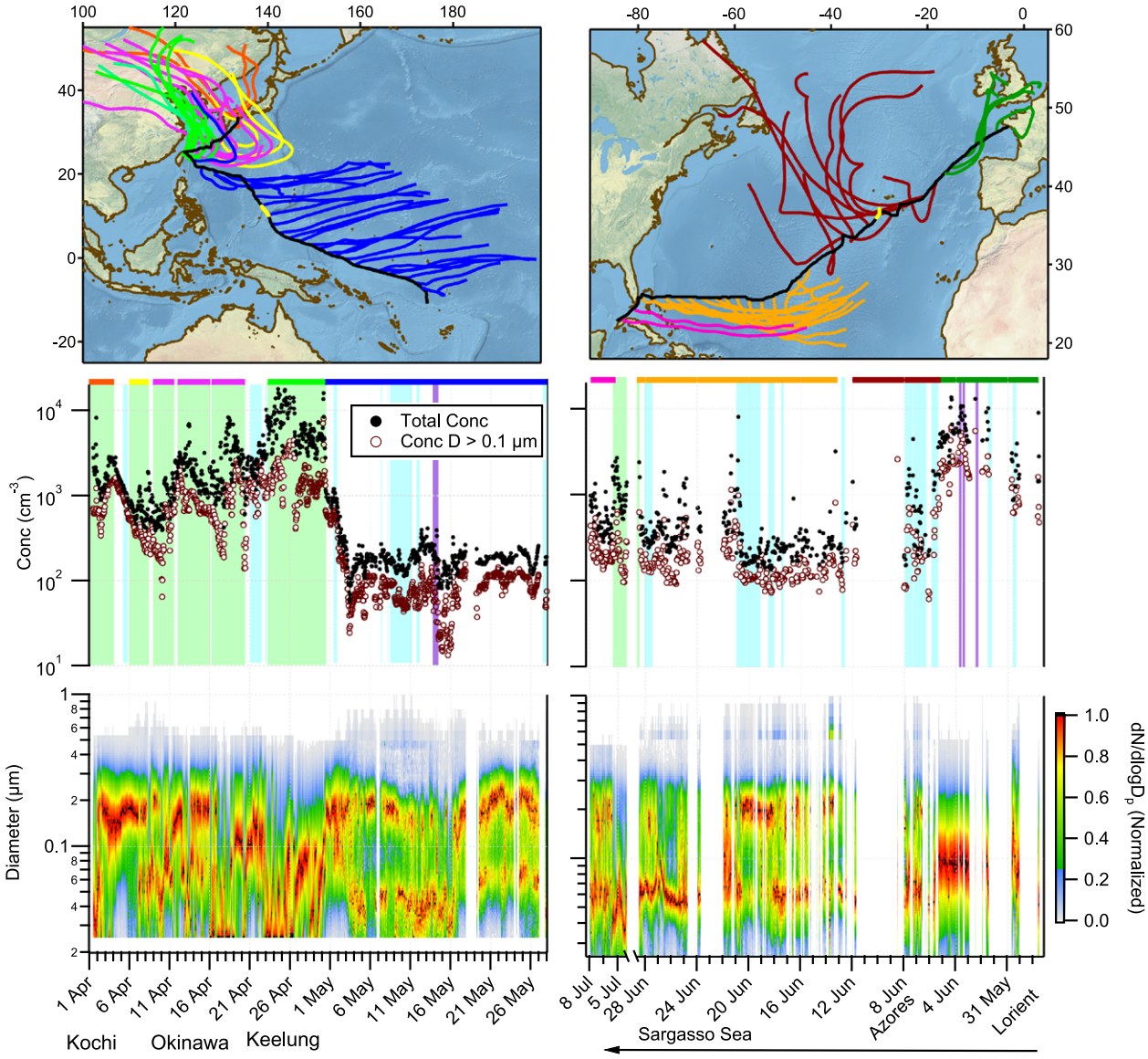

Fig. 3. Subsets from the full expedition of the time series of particle concentration and size distributions along the western Pacific and Atlantic Ocean crossings. The maps show *Tara*'s route (black line) and 48-h back trajectories along the route. To help with *Tara*'s location in time, the color bars above the time series panels correspond with the colors of the back trajectories. The light-blue columns show the periods where the engines were off while sailing, and the light-green columns when *Tara* was docked or anchored. Rain periods annotated by a crew member or scientist on board are marked with purple columns. The size distribution was normalized to the maximum concentration. The time axis in the Atlantic Ocean's data was reversed to coincide with the location in the map; the arrow below shows the direction the graph should be read. The yellow periods along the route correspond to the size distributions shown in Fig. 4b.

after the rainy day can be speculated to be the background pristine concentration in the marine boundary layer. On the other hand, in the Kochi–Keelung period, the total aerosol concentration rarely decreased below 1,000 cm^{-3}, the lowest concentration measured was in Iwo Tori Island (9 April 2017), 140 km north of Okinawa, with a concentration of 388 cm^{-3}. Even with air masses spending over 20 h above the ocean (up to 1,000 km from the coast), the aerosol concentration in the boundary layer is of a polluted atmosphere. For example, in the sailing period between Okinawa and Keelung (21–23 April) the average concentration is 2,718 (±1,560) cm^{-3}. Additionally, along this period the size distributions are mostly single-mode distributions with the modal diameter greater than 0.1 μm, with a few exceptions in Okinawa, 16–18 April, where the mode diameter is around 0.03 μm, and in Keelung, Taiwan,

where the mode diameters are in the Aitken mode. An interesting feature can be seen while *Tara* was leaving Keelung heading to the open ocean, first we see the continuous decrease in total aerosol concentration together with the transition from a single-mode distribution, to the clean marine aerosol size distribution (characterized by two modes); it took over 650 km to stop seeing the continental influence in the measurements.

The Atlantic Ocean, on the other hand, has a consistently higher number of aerosols compared to the Pacific. Figure 3 presents three types of trajectories: 1) with 48-h back trajectories of continental origin (green curves), 2) with the air masses coming from the North Atlantic (red curves), and 3) with easterly marine air masses (orange and pink curves). For the period where the air masses have some continental influence, we see total aerosol concentrations of over 5,000 cm^{-3} even 1,000 km away from the European continent and a consistent single-mode distribution around 0.1-μm mode diameter, only after the Azores the concentration decreased to values below 1,000 cm^{-3}. The period that is characterized by North Atlantic air masses has an average total aerosol concentration of 864 (±806) cm^{-3} and the transition from single-mode size distributions to double mode can be seen. Finally, the period with easterly back trajectories, has an average of 422 (±591) cm^{-3}, with a minimum measured value of 136 cm^{-3}. The size distribution fluctuates between a more pronounced accumulation mode (around 20 June) and a more pronounced Aitken mode (around 25 June).

Figure 4 shows an example summary of the differences in total aerosol concentration, an example of size distribution at similar wind speeds, and the source regions measured in the Atlantic crossing and the western Pacific Ocean. The open-ocean concentrations show a greater variation in the Atlantic than in the Pacific (Fig. 4a), along with a greater number of coarse-mode aerosol for the same wind speed (~11 m s^{-1}; Fig. 4b). The average wind speed in both the Atlantic and Pacific was around 6 m s^{-1} (5.6 ± 2.5 and 6.0 ± 2.7 m s^{-1}, respectively). The periods shown in Fig. 4 represent about 2% of the Atlantic measured data and 3% of the Pacific data. Scanning electron microscope (SEM) images of the filters collected concomitantly to the measured size distributions (Fig. 4b) show the differences in the type of coarse-mode aerosols present. In the Pacific Ocean sea salt was predominantly present, whereas mineral dust aerosol was found in the Atlantic Ocean filters. The energy disperse X-ray of these mineral dust particles showed no sodium present (although other mineral dust particles measured in the Caribbean Sea were found to be internally mixed with NaCl; see below). Additionally, the 48-h back trajectories show the air masses came from the north. Therefore, the presence of mineral dust of several microns in size without sodium present, implies continuous sedimentation from the free troposphere into the Atlantic Ocean marine boundary layer and its ocean surface.

Modal number fractions of marine aerosol size distributions. Recently, Modini et al. (2015) reported an approach to determine the SSA fraction from the total marine aerosol population using a lognormal-mode-fitting procedure, and Quinn et al. (2017) used this approach for several cruises along the Atlantic and Pacific Oceans. We used the fitting procedure described in Quinn et al. (2017) to determine the different fractions along the Atlantic and the west Pacific transects (Fig. 3; see appendix C for the methods description). We only focused on areas where R/V *Tara* was at least 100 km from the coasts and back trajectories spent over 24 h above the ocean. In general, three modes were fitted: one for the Aitken mode, one for the accumulation mode, and one for the SSA-mode aerosol [we use the same notation as was used in Quinn et al. (2017)], but for some periods in the Atlantic Ocean and the Caribbean Sea a fourth mode (referred to as "giant," with mode diameters, in general, >1 μm) was identified (e.g., see Fig. C1a). The number fraction of each mode was then calculated by taking the total number concentration in each lognormal fit mode and dividing by the sum of them (Fig. 5).

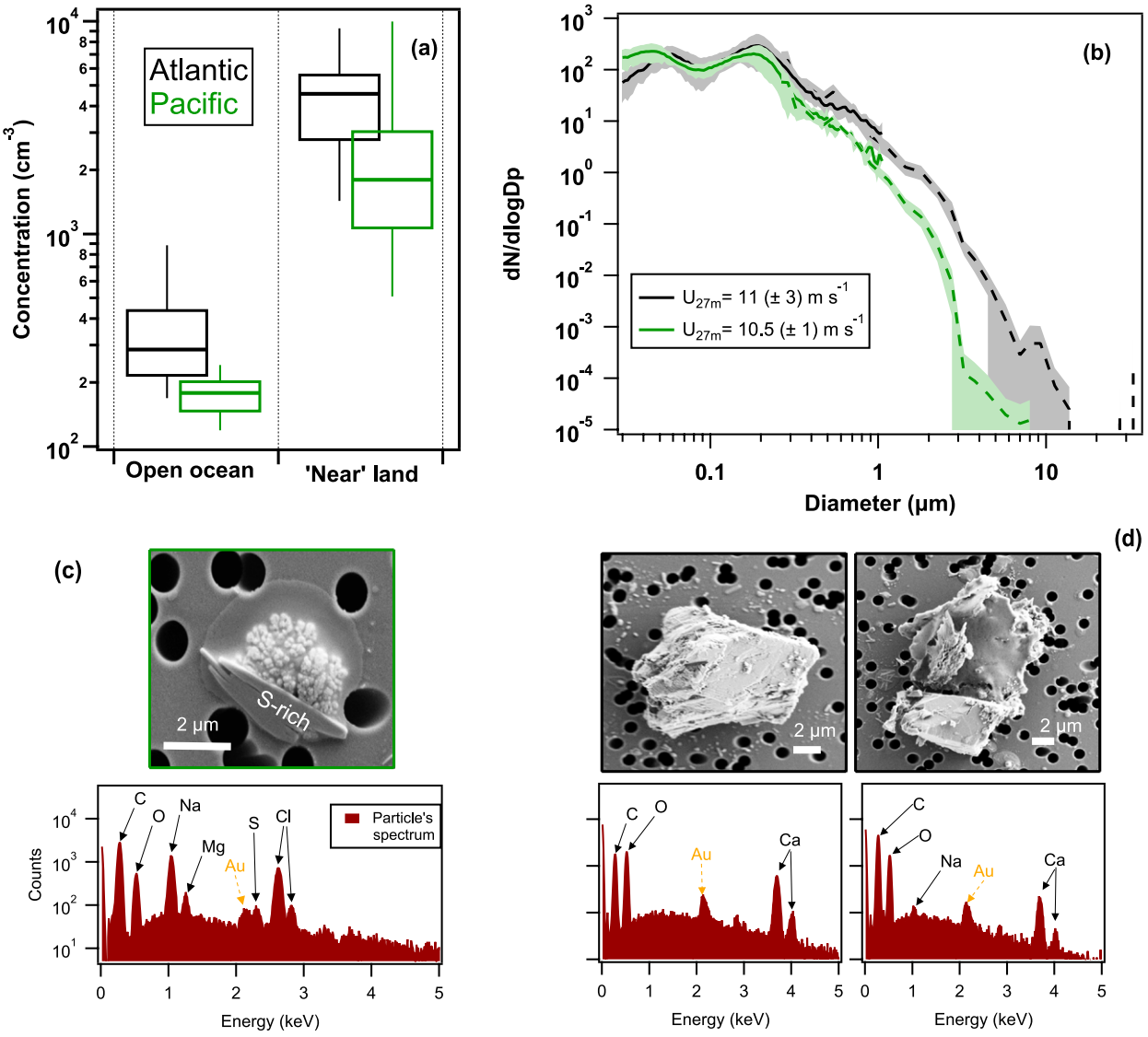

Fig. 4. Differences in concentration, size distribution, and composition between the Atlantic and Pacific Oceans. (a) Boxplot analysis of the total aerosol concentration in the open ocean (for the Pacific Ocean refers to the period between 3 and 26 May 2017, and for the Atlantic Ocean for the period between 6 and 27 Jun 2016), and near-continental sources (for the Pacific it refers to the period around Japan and Taiwan, 1 Apr to 1 May 2017, and for the Atlantic Ocean the period between France and the Azores, 28 May to 5 Jun 2016. (b) Aerosol size distribution for periods of ~16 h with similar wind speed of 11 m s^{-1}. The areas where the size distributions were measured are marked in yellow on the black sailing path in Fig. 3. (c) SEM image of a representative Pacific Ocean particle (9–10 May 2017) found in the same period as the size distributions from (b). The energy-dispersive X-ray spectrum are shown below the SEM images. (d) As in (c), but for the Atlantic Ocean (7 Jun 2016).

A summary of the ranges in the geometric mean diameter (GMD) and the geometric standard deviation, for the Aitken, accumulation, SSA, and giant aerosol modes are listed in Table 1. The Aitken and accumulation modes varied similarly in the western Pacific (Fig. 5a), the Atlantic Oceans, and the Caribbean Sea (Fig. 5c), with GMD values ranging from 0.04 to 0.09 μm in the Aitken mode and 0.14 to 0.22 μm in the accumulation mode. On the other hand, there are more variations in the SSA mode in the Atlantic Ocean, with GMD values varying from 0.18 to 0.51 μm, compared to the Pacific Ocean where the GMD values mostly varied around 0.35 to 0.52 μm, with a few cases where the GMD decreased to values around 0.21–0.24 μm. The giant aerosol mode was only observed in the Atlantic Ocean and the Caribbean Sea, with GMD values ranging between 1.0–1.9 μm and

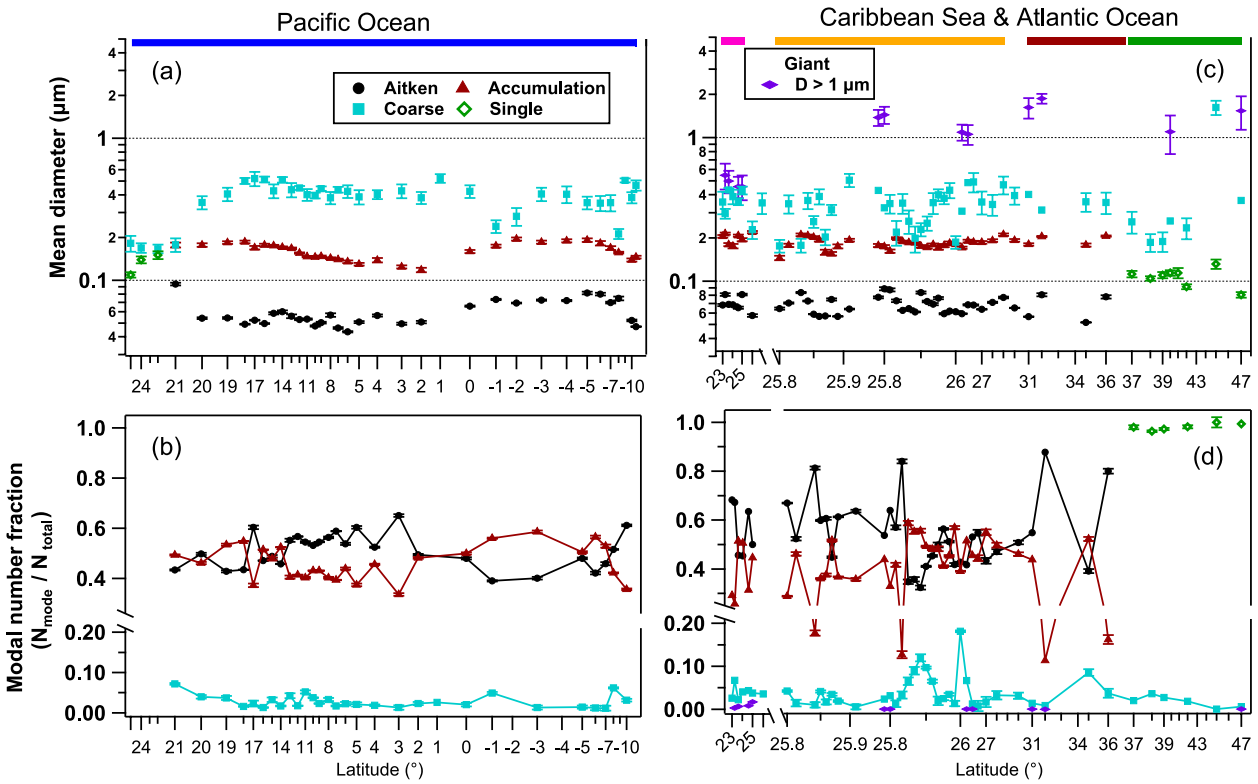

Fig. 5. (top) Mode diameters and (bottom) number fraction of the lognormal fits. "Single" refers to a single lognormal distribution fitted for the Aitken and accumulation modes. The error bars are one standard deviation.

Table 1. Range of the geometric mean diameters, geometric standard deviation, and modal fractions of the total number of marine aerosols from the lognormal fits of the marine aerosol number size distributions measured across the Atlantic and Pacific Oceans. The average wind speed for each period is shown on the rightmost column.

		Geometric mean diameters (D_g, μm), geometric standard deviation (σ_g), and number fraction (%)												
		Aitken			Accumulation			Coarse			Giant			
	Lat, lon	D_g	σ_g	Fraction	D_g	σ_g	Fraction	D_g	σ_g	Fraction	D_g	σ_g	Fraction	Avg wind speed m s^{-1}
Atlantic Ocean (before Azores)	47°N, 3.9°W to 37°N, 24.8°W	Single mode distribution 0.08–0.13 (1.7–2.1)						0.19–0.36	0.8–2.2	0–4	1.1–1.5	0.7–1.6	<0.01	5.3 (±1.9)
Atlantic Ocean	36°N, 28.3°W to 25.8°N, 80°W	0.05–0.09	0.6–2.0	32–88	0.14–0.21	0.6–1.5	11–59	0.18–0.51	0.5–2.3	1–18	1.0–1.9	0.7–1.3	<0.1	5.8 (±2.6)
Caribbean Sea	25.8°N, 80°W to 23°N, 84°W	0.06–0.08	1.5–1.7	45–68	0.17–0.22	0.8–1.5	26–52	0.23–0.43	1.5–2.0	2–7	0.45–0.55	0.5–0.6	0.3–2	5.9 (±1.7)
Pacific Ocean	21°N, 126°E to 11°S, 174°E	0.04–0.09	1.0–1.9	39–65	0.12–0.19	0.7–1.6	34–59	0.21–0.52	0.4–2.0	1–7				6.0 (±2.7)

0.45–0.55 μm, respectively. This giant mode can be attributed to dust sedimentation from the free troposphere.

The number fraction for the SSA mode in the Pacific Ocean (Fig. 5b) did not exceed 7%. The Aitken and accumulation modes changed latitudinally. While between 14° and 1°N the Aitken mode dominated, with 55%–65% of the total fraction, between the equator and 7°S the accumulation mode dominated with 50%–53% of the total fraction. These fractions are similar to the fractions reported by Quinn et al. (2017), where they reported ~51% fractions of the Aitken mode between 10°N and 10°S. The comparable fractions in the tropics result from the long aerosol residence times, caused by the consistent marine air masses and persistent trade winds flow (see the calculated back trajectories in the map of Fig. 3). This allows the growth of Aitken mode particles to accumulation mode sizes by cloud processing or vapor deposition processes (Hoppel et al. 1986; Covert et al. 1996). On the other hand, in the Atlantic Ocean, there are occasions when the SSA fraction reached 18% and in most of the transect, the Aitken mode had a larger fraction, occasionally reaching 88%. Between 31° and 26°N the Aitken and accumulation modes had similar number fractions around 50%, while in the last part of the Atlantic crossing, with the R/V *Tara* remaining around 26°N, the Aitken-mode fraction was consistently higher than the accumulation mode, with values ranging between 54% and 67%. Quinn et al. (2017) found highly variable Aitken- and accumulation-mode fractions between 20° and 40°N, while the SSA mode made up 15% or less across all latitudes, from 70°S to 80°N.

Morphology and elemental analysis. Single-particle analysis is a powerful tool for studying chemical reactions, sources and formation mechanisms, hygroscopicity and the environmental impact on the collected aerosols. We used SEM, in combination with energy dispersive X-ray (Bruker XFlash 60 mm) analysis (SEM-EDX) to determine the composition and size of individual particles with diameters down to about 0.8 μm (see appendix D). This analysis is planned to be applied to all the filters that were collected along the 2.5 years, but at this stage, we can present here some examples from the Pacific Ocean and the Caribbean Sea. One goal of this analysis is to identify major mineral composition in marine aerosol and to determine whether and how they are aggregated with other aerosol species, and to identify the aggregated species. For example, Fig. 6 shows three mineral dust particles collected west of Cuba (23°N, 85°W) with its corresponding X-ray spectrum. Internal mixtures of silicate with sodium chloride and $CaSO_4$ were identified in different ratios and sizes. The collected mineral dust was transported through Cuba where 76 and 98 kilotons yr^{-1} of SO_2 can be produced (Fioletov et al. 2016), hence it is likely the primary emitted anhydrite reacted with SO_2 (Buseck and Pósfai 1999) serving as an SO_2 removal pathway (Dentener et al. 1996). The internal mixtures observed in Fig. 6 of NaCl, sulfate, and $CaSO_4$ were previously observed and are thought to be formed in clouds (Andreae et al. 1986). Cloud processing has been observed to convert mineral dust into giant CCN and influence precipitation and ice crystal concentration in convective clouds (Levin 2005).

Another goal of the single-particle analysis is to identify crystallization differences in sea salt aerosols' internal mixtures. Such information is useful for obtaining improved refractive indices, shape and size data for model calculations of the radiative forcing of dust and SSA. Additionally, the observation of internal or external mixtures is important for determining which chemical reactions take place and how primary aerosol particles change during atmospheric transport. Figure 7 shows four examples of crystallized sea salt aerosols with identical EDX spectra collected in the western Pacific Ocean on 12 May 2017 (10°N, 141°E). The spectra below the images in Fig. 7 shows the average of the four particles' spectra along each particle's spectrum. The four particles show a disk surrounding them. These disks are likely residues of organic material present in the sea surface microlayer or scavenged by bubbles rising to

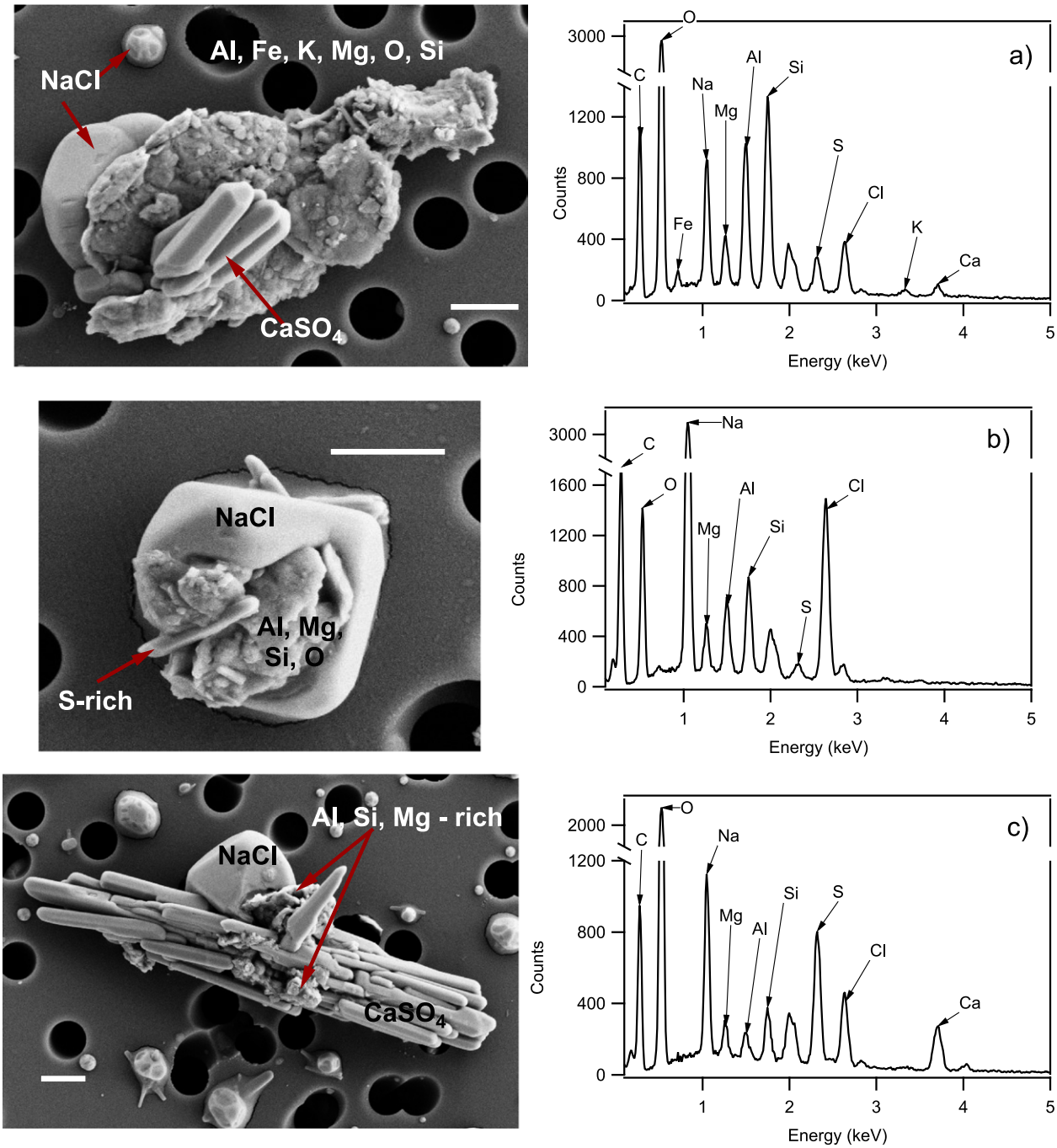

Fig. 6. SEM images of mineral dust particles collected west of Cuba. The corresponding X-ray spectra are shown on the right. The size bar is 1 μm.

the air–sea interface, since sea salt particles are formed when rising bubbles, produced by breaking waves, burst and create film and jet droplets at the ocean–atmosphere interface (Day 1964; Blanchard 1963; Wu 1981). Sea salt particles dominate the particulate surface area in the marine atmosphere, making them the main light scatterer over the oceans, one of the dominant sources of aerosol mass, and important component in the atmospheric cycles of Cl, S, and N (Buseck and Pósfai 1999; Lewis and Schwartz 2004). Although it was recently estimated to account for less than 30% of the total amount of marine CCN (Quinn et al. 2017), sea salt particles serve as good CCN and have a significant role in determining the size distribution and number concentration of drops in marine clouds (Feingold et al. 1999; Gantt et al. 2012; McCoy et al. 2015), and recently it was shown that they can be used as a tool to study wet removal of aerosols (Murphy et al. 2019). Individual particle analysis can be used to

determine the emitted sea salt's shape and internal mixing composition (e.g., its sulfate concentrations and sizes) to better understand the radiative impact by constraining its optical properties and CCN contribution.

Biological properties of marine aerosols. Our understanding of how ocean microbiology affects SSA emission and properties is still rudimentary. It has been acknowledged that one of the main factors affecting SSA abundance and chemical composition is biological activity in the oceanic microlayer and mixed layer (Facchini et al. 2008; Quinn et al. 2015). Additionally, the chemical composition and size distribution of oceanic CCN, are not only influenced by the abundance of organic matter in the seawater but are significantly affected by the composition of the planktonic ecosystem (Lee et al. 2015; Prather et al. 2013). One of the major challenges is to understand which type of microorganisms, viruses, and bacteria are emitted from the marine environment, which ones remain viable after redeposition, which ones are transported from continental areas, and what is their impact on the marine environment. There are very few studies on the abundance of microbes in the atmosphere of the open ocean (Mayol et al. 2017, 2014; Burrows et al. 2009b). Burrows et al. (2009a) estimated 40–1,800 Gg dry weight yr^{-1} of bacteria emission to the atmosphere and Mayol et al. (2017) estimated around 2.2×10^{21} and 2.1×10^{21} of prokaryotic and eukaryotic cells, respectively, in the open ocean with 33%–68% having marine origin. Understanding what role oceans play as a source and sink of microorganisms (viruses and bacteria), and their atmospheric transport can provide important insights on microbial diversity and the interplay between terrestrial communities and their spread over oceanic regions.

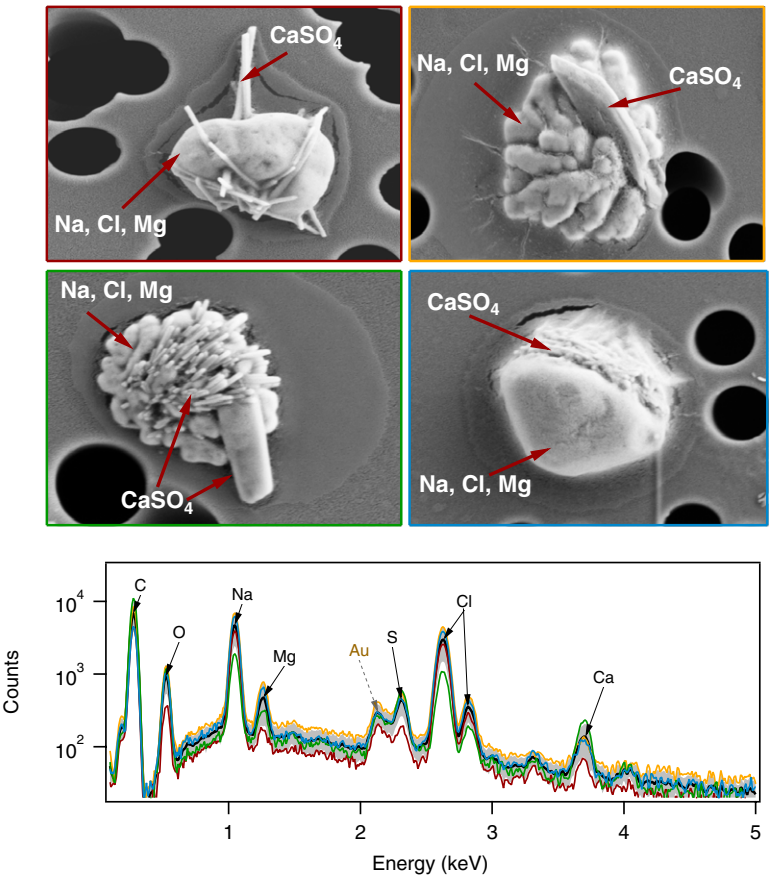

Fig. 7. SEM images of sea salt particles collected in the western Pacific Ocean. The four particles had similar X-ray spectra, shown below the images. The color of the frame of each SEM image corresponds to the color of the X-ray spectrum trace; the average of them is shown in black with the standard deviation shown as a shaded gray area. The black holes are 0.8 μm in diameter.

We collected over 1,000 air filter samples which will be analyzed for microbial biodiversity using marker gene sequencing of the small bacterial (16S) and eukaryote (18S) ribosomal subunit. Using this data, along with a comparison with the microbiome composition of the surface ocean data (Gorsky et al. 2019), we will be able to correlate between the microbial and chemical composition of the SSA and open-ocean sea surface water.

Summary and outlook

We presented here a new set of marine aerosol measurements done as part of the *Tara* Pacific Expedition along the Atlantic and Pacific Oceans. These measurements done in parallel with surface-water measurements (Gorsky et al. 2019) will help us to better understand processes and feedbacks of the coupled ocean–atmosphere system and will enable the building of a

new dataset that describes in detail marine aerosol properties. Preliminary results of aerosol concentrations and size distributions were presented here (and summarized below). Future analyses are listed as well as their potential to answer questions related to marine aerosol chemical and optical properties, aerosol production mechanisms and the link to environmental conditions and marine biology.

The size distribution analysis of the marine aerosols across the western Pacific Ocean showed there is an average total aerosol concentration of 180 (±51) cm^{-3} in the open ocean (far from land), with an average of 83 (±30) cm^{-3} for aerosol with diameters greater than 0.1 μm (potential CCN) with most of the transect characterized by a bimodal distribution. A daylong rain period revealed that a pristine marine atmosphere can have total aerosol concentration as low as 82 cm^{-3} (with 13 cm^{-3} for $D > 0.1$ μm) and has a single Aitken-mode distribution with a mode diameter of around 0.031 μm. Continental influence was recognized up to 650 km away from the coast.

In the Atlantic Ocean, there was a consistently higher concentration of aerosols. Between the European continent and the Azores, concentrations of over 5,000 cm^{-3} characterized by a single accumulation-mode distribution were measured, even 1,000 km away from the European continent. In the open Atlantic Ocean, between the Azores and the city of Miami, with airmass back trajectories of marine origin, concentration values varied between 136 cm^{-3} and over 1,000 cm^{-3}. The presence of mineral dust on the Atlantic Ocean filters and the appearance of a giant mode in the modal fraction analysis, suggest sedimentation of mineral dust from the free troposphere into the marine boundary layer and its ocean surface.

The SSA contribution to the total aerosol population in the Pacific Ocean (Fig. 6b) did not exceed 7%, while in the Atlantic Ocean there are occasion the SSA fraction reached 18% and in most of the transect the Aitken mode had a larger fraction, on occasions reaching 88%.

The information gained from the size distributions will help us identify areas of interest that can be studied thoroughly for aerosol production mechanisms using satellite measurements, reanalysis meteorological data and other onboard oceanic measurements (e.g., chlorophyll *a* concentrations, sea surface temperature, particulate organic carbon).

The image and single-particle analyses showed a wide variety of internal mixtures: silicates with sodium chloride and $CaSO_4$ in mineral dust, as well as the difference in shape sea salt aerosol can acquire when crystallizing after drying. The SEM-EDX analysis will be further used to quantify the size, shape, quantity, and elemental composition of all aerosols greater than 0.8 μm.

The biomass from the filters will be extracted to assess for microbial diversity metagenomics, 16S and 18S sequencing. Pattern of microbial diversity and abundances will then be compared to the oceanic population and compared with other parameters in order to give a comprehensive overview of the potential biological microbial exchange between the ocean and the atmosphere.

The same atmospheric measurement setting will stay as a permanent component of future *Tara* missions. With such measurements we expect to better understand feedbacks between marine ecology, mixed layer and microlayer properties, aerosols, and clouds, in different natural and anthropogenic environments.

Acknowledgments. Special thanks to the Tara Ocean Foundation, the R/V *Tara* crew and the *Tara* Pacific Expedition Participants (https://doi.org/10.5281/zenodo.3777760). This research was supported by a research grant from Scott Jordan and Gina Valdez, the De Botton center for Marine Science, the Yeda-Sela center for Basic research, and a research grant from the Yotam Project.

We are keen to thank the commitment of the following institutions for their financial and scientific support that made this unique *Tara* Pacific Expedition possible: CNRS, PSL, CSM, EPHE, Genoscope/

CEA, Inserm, Université Côte d'Azur, ANR, agnès b., UNESCO-IOC, the Veolia Foundation, the Prince Albert II de Monaco Foundation, Région Bretagne, Billerudkorsnas, Amerisource Bergen Company, Lorient Agglomeration, Oceans by Disney, L'Oréal, Biotherm, France Collectivités, Fonds Français pour l'Environnement Mondial (FFEM), Etienne Bourgois, and the Tara Ocean Foundation teams. *Tara* Pacific would not exist without the continuous support of the participating institutes. The authors also particularly thank Serge Planes, Denis Allemand, and the *Tara* Pacific consortium. This study has been conducted using E.U. Copernicus Marine Service Information and Mercator Ocean products. FL is supported by Sorbonne Université, Institut Universitaire de France and the Fondation CA-PCA. The in-line and oceanic optics dataset was collected and analyzed with support from NASA Ocean Biology and Biogeochemistry program under Grants NNX13AE58G and NNX15AC08G to the University of Maine. This is publication number 9 of the *Tara* Pacific Consortium.

The authors gratefully acknowledge the NOAA Air Resources Laboratory (ARL) for the provision of the HYSPLIT transport and dispersion model and/or READY website (www.ready.noaa.gov) used in this publication.

All data for this article will be deposited in PANGEA-Data Publisher for Earth and Environmental Science. They are also available upon request to the corresponding author.

Appendix A: Inlet system

Two inlet systems were constructed using funnels as the inlets heads and with silicone conductive tubing of 1.9-cm inner diameter. One inlet system was connected from the funnel to the SMPS–OPC system and the second inlet system to the home-built aerosol filter system. For the first Atlantic crossing, the tubing was about 15 m in length and for the rest of the expedition approximately 27 m. The SMPS–OPC and the home built aerosol filter system were installed in the stern of the boat for the whole expedition.

Due to the structure of *Tara* (i.e., a schooner built to do an arctic drift), to be able to measure consecutively for 2.5 years in remote areas, and since the only place to install the inlets was along the backstay, we used funnels as our inlets. The funnels were directed down to prevent rain from entering and to not bias sampling in one direction. We did not implement any size cutoff mechanism; we measured bulk aerosol. We did not implement an automatic shutoff of the system. Engine contamination periods were handled as described in appendix B for the size distribution measurements. For the filters, we used the identified contamination periods and marked the corresponding filters; these filters will not be used for chemical analysis.

Separate particle loss calculations (using the Particle Loss Calculator; Von der Weiden et al. 2009) were done for the first Atlantic crossing and the rest of the campaign due to the differences in height of the inlet (Fig. A1).

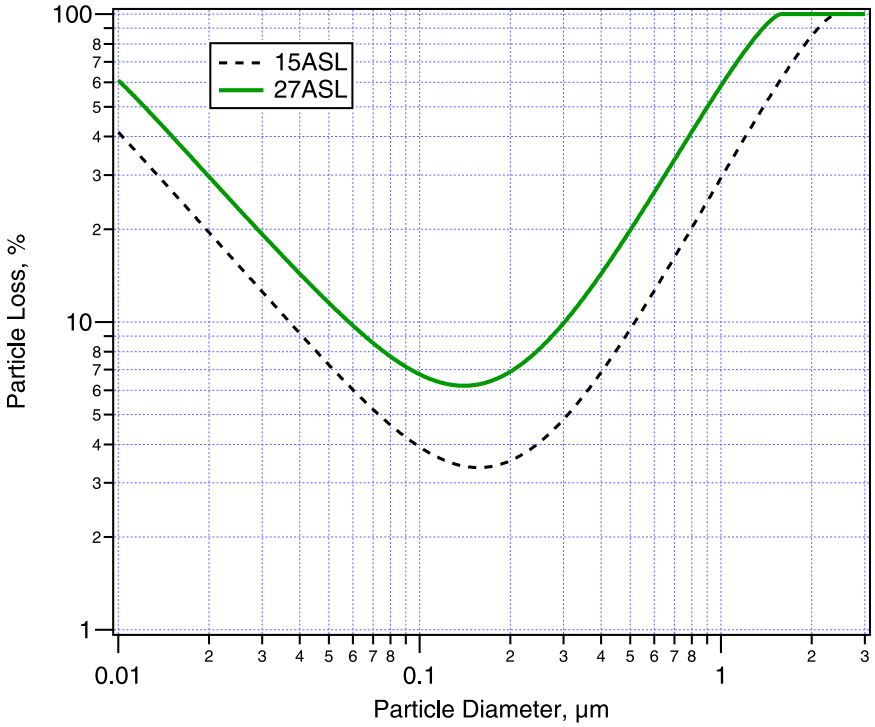

Fig. A1. Theoretical particle loss through the inlets installed on the back stay of *Tara*. The calculations were done using the Particle Loss Calculator (Von der Weiden et al. 2009).

For the SMPS–OPC system, a Nafion dryer was installed before it. The relative humidity (RH) was measured after the Nafion dryer, and before each SMPS scan. For the Atlantic crossing the average RH was measured to be 35% (±5%). For the Keelung–Fiji transect, the average RH was measured to be 37% (±4%).

An extra diffusion dryer was installed between the Nafion and the SMPS to further dry the air before entering the SMPS. The RH values (after this diffusion dryer) could not be measured continuously, it was measured at the beginning of the expedition and it was found to reduce the RH to about 10% when the silica gel beads where newly changed.

Appendix B: Marine aerosol size distribution corrections

For an accurate representation of the marine size distributions, three steps were taken for the SMPS–OPC data. First, engine contamination periods were identified. Taking advantage that the R/V *Tara* is a schooner, the engines were only turned on when necessary. These periods were recorded by the crew and were used as the first filter to detect possible contamination periods. If a drastic increase was identified in the transitions from sailing to engines on, the data were excluded. Additionally, contamination periods were identified in the SMPS–OPC system as a single-mode size distribution with a mode diameter of less than 0.04 μm and total particle concentrations on the order of 10^5 cm^{-3}. Contamination periods were identified only in the first Atlantic crossing and were excluded from the analysis. Next, the size distributions were corrected for the estimated particle loss through the inlets (see appendix A). Finally, to correct for possible biases due to the OPC refractive index calibration, the OPC data were corrected using the overlap region of the SMPS and merged to obtain a total aerosol size distribution from 0.03 to 32 μm. The overlap region used was between 0.3 and 0.7 μm, which includes eight overlapping bins of the OPC. The limits of both instruments were avoided. We used a method similar to the one described by Hand and Kreidenweis (2002) to merge the SMPS and OPC overlap regions. In short, the SMPS data were used to "calibrate" the OPC data, but we do not use it to derive refractive indices nor density. The method assumes spherical particles and internal particle mixture over the overlap region used.

Appendix C: Calculation of different mode fractions

To calculate the modal number fractions, the data were averaged in 1° latitude or longitude bins (within each latitude or longitude bin there are at least 8 h of measurements). The size distributions were then used to calculate the different mode fractions by fitting multiple lognormal modes, up to four lognormal distributions, using the lognormal fit function in IGOR Pro (Wavemetrics) (Fig. C1). A chi-square test was used to assess the multimodal fit reproduced the measured size distribution. A significance level of 0.05 was used as the critical value, and only those with the chi-square value less than 0.05 were used in the analysis.

Appendix D: Scanning electron microscope with energy disperse x-ray analysis

To perform the SEM-EDX analysis, first, the filters are coated with either AuPd or Ir, then a chosen particle is imaged and finally, a full image X-ray scan is performed. The X-ray scan is at least 5 min long at 1,000 counts s^{-1} using a 7–10 keV accelerating voltage.

The EDX spectra shown here (Figs. 4, 6, and 7) are extracted by choosing only the area of the individual particle.

Appendix E: *Tara* Ocean Foundation

More information on the *Tara* Ocean Foundation (https://oceans.taraexpeditions.org) and the *Tara* Pacific Expedition (https://oceans.taraexpeditions.org/en/m/about-tara/les-expeditions/tara-pacific/) can be found online.

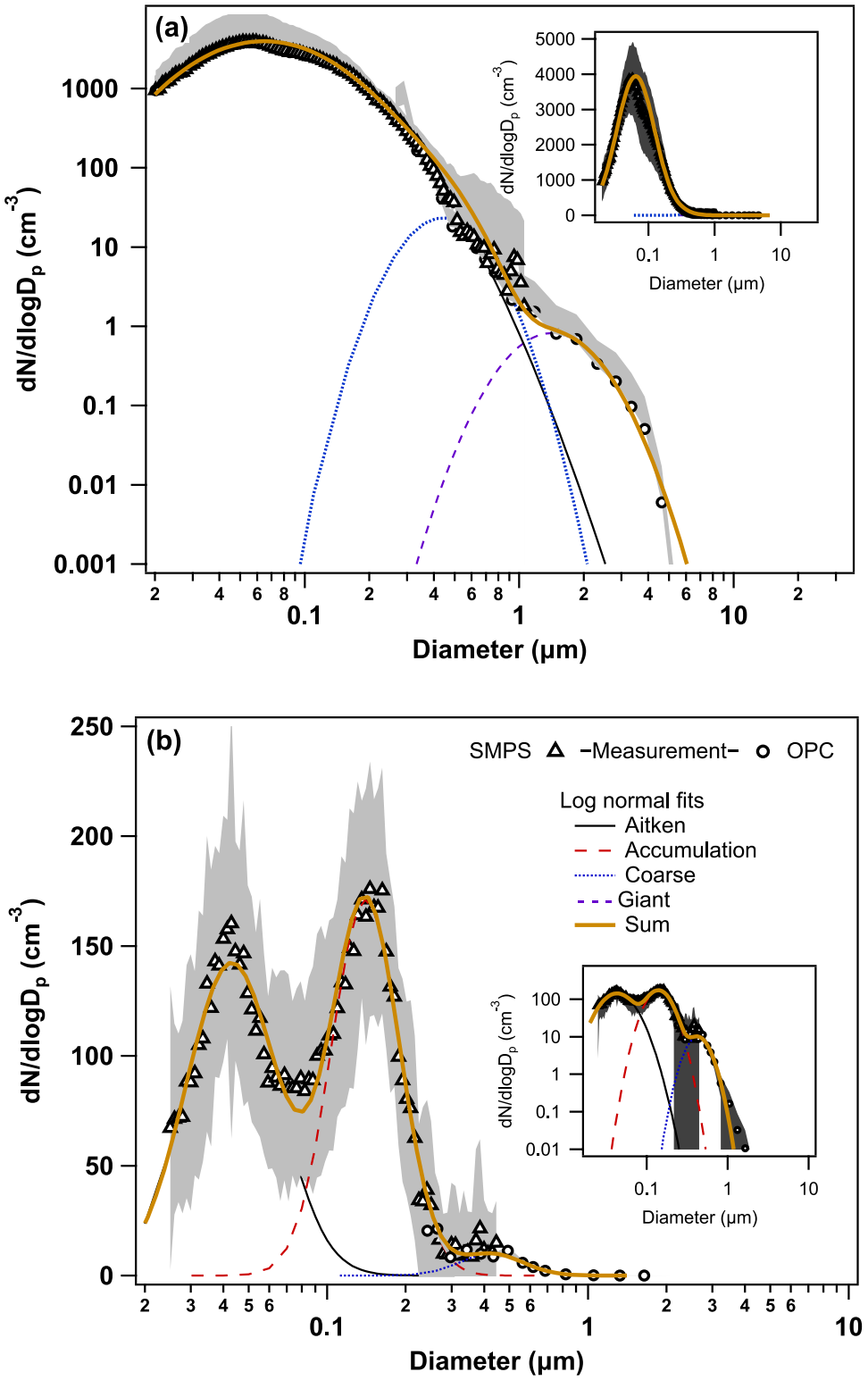

Fig. C1. Two examples of the fitted lognormal modes on measured particle size distribution. (a) Log–log scale of the marine aerosol size distribution measured on 30 May 2016 in the Bay of Biscay showing a "giant" mode in the marine aerosol. A single lognormal distribution was fitted to the measured distribution below 0.4 μm (black line). The gray shaded area is the standard deviation of the average, and only the upper region is shown for clarity. The large errors in the overlap region come from the SMPS low resolution in that region. (b) Log–linear scale of the marine aerosol size distribution measured on 10 May 2017 in the western Pacific Ocean. The inset shows the log–log scale. The size distributions were averaged over 1° latitude or longitude.

References

Andreae, M. O., R. J. Charlson, F. Bruynseels, H. Storms, R. VAN Grieken, and W. Maenhaut, 1986: Internal mixture of sea salt, silicates, and excess sulfate in marine aerosols. *Science*, **232**, 1620–1623, https://doi.org/10.1126/SCIENCE.232.4758.1620.

Ben-Ami, Y., I. Koren, O. Altaratz, A. Kostinski, and Y. Lehahn, 2012: Discernible rhythm in the spatio/temporal distributions of transatlantic dust. *Atmos. Chem. Phys.*, **12**, 2253–2262, https://doi.org/10.5194/acp-12-2253-2012.

Betzer, P. R., and Coauthors, 1988: Long–range transport of giant mineral aerosol particles. *Nature*, **336**, 568–571, https://doi.org/10.1038/336568a0.

Blanchard, D. C., 1963: The electrification of the atmosphere by particles from bubbles in the sea. *Prog. Oceanogr.*, **1**, 73–202, https://doi.org/10.1016/0079-6611(63)90004-1.

Boucher, O., and Coauthors, 2013: Clouds and aerosols. *Climate Change 2013: The Physical Science Basis*, T. F. Stocker et al., Eds., Cambridge University Press, 571–657.

Brooks, S. D., and D. C. O. Thornton, 2018: Marine aerosols and clouds. *Annu. Rev. Mar. Sci.*, **10**, 289–313, https://doi.org/10.1146/annurev-marine-121916-063148.

Burrows, S. M., T. Butler, P. Jöckel, H. Tost, A. Kerkweg, U. Pöschl, and M. G. Lawrence, 2009a: Bacteria in the global atmosphere–Part 2: Modeling of emissions and transport between different ecosystems. *Atmos. Chem. Phys.*, **9**, 9281–9297, https://doi.org/10.5194/acp-9-9281-2009.

——, W. Elbert, M. G. Lawrence, and U. Pöschl, 2009b: Bacteria in the global atmosphere–Part 1: Review and synthesis of literature data for different ecosystems. *Atmos. Chem. Phys.*, **9**, 9263–9280, https://doi.org/10.5194/acp-9-9263-2009.

Buseck, P. R., and M. Pósfai, 1999: Airborne minerals and related aerosol particles: Effects on climate and the environment. *Proc. Natl. Acad. Sci. USA*, **96**, 3372–3379, https://doi.org/10.1073/pnas.96.7.3372.

Carslaw, K. S., and Coauthors, 2017: Aerosols in the pre-industrial atmosphere. *Curr. Climate Change Rep.*, **3**, 1–15, https://doi.org/10.1007/s40641-017-0061-2.

Charlson, R. J., J. E. Lovelock, M. O. Andreae, and S. G. Warren, 1987: Oceanic phytoplankton, atmospheric sulphur, cloud albedo and climate. *Nature*, **326**, 655–661, https://doi.org/10.1038/326655a0.

Covert, D. S., V. N. Kapustin, T. S. Bates, and P. K. Quinn, 1996: Physical properties of marine boundary layer aerosol particles of the mid-Pacific in relation to sources and meteorological transport. *J. Geophys. Res.*, **101**, 6919–6930, https://doi.org/10.1029/95JD03068.

Day, J. A., 1964: Production of droplets and salt nuclei by the bursting of air-bubble films. *Quart. J. Roy. Meteor. Soc.*, **90**, 72–78, https://doi.org/10.1002/qj.49709038307.

De Leeuw, G., E. L. Andreas, M. D. Anguelova, C. W. Fairall, E. R. Lewis, C. O'Dowd, M. Schulz, and S. E. Schwartz, 2011: Production flux of sea spray aerosol. *Rev. Geophys.*, **49**, RG2001, https://doi.org/10.1029/2010RG000349.

——, and Coauthors, 2014: Ocean–atmosphere interactions of particles. *Ocean-Atmosphere Interactions of Gases and Particles*, P. S. Liss and M. T. Johnson, Eds., Springer, 171–246.

Dentener, F. J., G. R. Carmichael, Y. Zhang, J. Lelieveld, and P. J. Crutzen, 1996: Role of mineral aerosol as a reactive surface in the global troposphere. *J. Geophys. Res.*, **101**, 22 869–22 889, https://doi.org/10.1029/96JD01818.

Deschamps, P.-Y., B. Fougnie, R. Frouin, P. Lecomte, and C. Verwaerde, 2004: SIMBAD: A field radiometer for satellite ocean-color validation. *Appl. Opt.*, **43**, 4055, https://doi.org/10.1364/AO.43.004055.

Duce, R. A., C. K. Unni, B. J. Ray, J. M. Prospero, and J. T. Merrill, 1980: Long-range atmospheric transport of soil dust from Asia to the tropical North Pacific: Temporal variability. *Science*, **209**, 1522–1524, https://doi.org/10.1126/science.209.4464.1522.

Dusek, U., and Coauthors, 2006: Size matters more than chemistry for cloud-nucleating ability of aerosol particles. *Science*, **312**, 1375–1378, https://doi.org/10.1126/science.1125261.

Facchini, M. C., and Coauthors, 2008: Primary submicron marine aerosol dominated by insoluble organic colloids and aggregates. *Geophys. Res. Lett.*, **35**, https://doi.org/10.1029/2008GL034210.

Feingold, G., W. R. Cotton, S. M. Kreidenweis, and J. T. Davis, 1999: The impact of giant cloud condensation nuclei on drizzle formation in stratocumulus: Implications for cloud radiative properties. *J. Atmos. Sci.*, **56**, 4100–4117, https://doi.org/10.1175/1520-0469(1999)056<4100:TIOGCC>2.0.CO;2.

Fioletov, V. E., C. A. McLinden, N. Krotkov, C. Li, J. Joiner, N. Theys, S. Carn, and M. D. Moran, 2016: A global catalogue of large SO2 sources and emissions derived from the Ozone Monitoring Instrument. *Atmos. Chem. Phys.*, **16**, 11 497–11 519, https://doi.org/10.5194/acp-16-11497-2016.

Gantt, B., and Coauthors, 2012: Global distribution and climate forcing of marine organic aerosol–Part 2: Effects on cloud properties and radiative forcing. *Atmos. Chem. Phys.*, **12**, 6555–6563, https://doi.org/10.5194/acp-12-6555-2012.

Gorsky, G., and Coauthors, 2019: Expanding Tara Oceans protocols for underway, ecosystemic sampling of the ocean-atmosphere interface during Tara Pacific expedition (2016–2018). *Front. Mar. Sci.*, **6**, 750, https://doi.org/10.3389/fmars.2019.00750.

Hand, L., and M. Kreidenweis, 2002: A new method for retrieving particle refractive index and effective density from aerosol size distribution data. *Aerosol Sci. Technol.*, **36**, 1012–1026, https://doi.org/10.1080/02786820290092276.

Heintzenberg, J., D. C. Covert, and R. V. Dingenen, 2000: Size distribution and chemical composition of marine aerosols: a compilation and review. *Tellus B: Chem. Phys. Meteor.*, **52**, 1104–1122, https://doi.org/10.3402/tellusb.v52i4.17090.

Hoppel, W. A., G. M. Frick, and R. E. Larson, 1986: Effect of nonprecipitating clouds on the aerosol size distribution in the marine boundary layer. *Geophys. Res. Lett.*, **13**, 125–128, https://doi.org/10.1029/GL013i002p00125.

Jaeglé, L., P. K. Quinn, T. S. Bates, B. Alexander, and J.-T. Lin, 2011: Global distribution of sea salt aerosols: new constraints from in situ and remote sensing observations. *Atmos. Chem. Phys.*, **11**, 3137–3157, https://doi.org/10.5194/acp-11-3137-2011.

Kinne, S., and Coauthors, 2006: An AeroCom initial assessment – Optical properties in aerosol component modules of global models. *Atmos. Chem. Phys.*, **6**, 1815–1834, https://doi.org/10.5194/acp-6-1815-2006.

Lee, Y. H., P. J. Adams, and D. T. Shindell, 2015: Evaluation of the global aerosol microphysical ModelE2-TOMAS model against satellite and ground-based observations. *Geosci. Model Dev.*, **8**, 631–667, https://doi.org/10.5194/gmd-8-631-2015.

Levin, Z., 2005: On the interactions of mineral dust, sea-salt particles, and clouds: A measurement and modeling study from the Mediterranean Israeli dust experiment campaign. *J. Geophys. Res.*, **110**, D20202, https://doi.org/10.1029/2005JD005810.

Lewis, R., and E. Schwartz, 2004: *Sea Salt Aerosol Production: Mechanisms, Methods, Measurements and Models—A Critical Review. Geophys. Monogr.*, Vol. 152, Amer. Geophys. Union, 413 pp.

Martin, J. H., and Coauthors, 1994: Testing the iron hypothesis in ecosystems of the equatorial Pacific Ocean. *Nature*, **371**, 123–129, https://doi.org/10.1038/371123a0.

Mayol, E., M. A. Jiménez, G. J. Herndl, C. M. Duarte, and J. M. Arrieta, 2014: Resolving the abundance and air-sea fluxes of airborne microorganisms in the North Atlantic Ocean. *Front. Microbiol.*, **5**, 557, https://doi.org/10.3389/fmicb.2014.00557.

——, and Coauthors, 2017: Long-range transport of airborne microbes over the global tropical and subtropical ocean. *Nat. Commun.*, **8**, 201, https://doi.org/10.1038/s41467-017-00110-9.

McCoy, D. T., S. M. Burrows, R. Wood, D. P. Grosvenor, S. M. Elliott, P.-L. Ma, P. J. Rasch, and D. L. Hartmann, 2015: Natural aerosols explain seasonal and spatial patterns of Southern Ocean cloud albedo. *Sci. Adv.*, **1**, e1500157, https://doi.org/10.1126/sciadv.1500157.

Middleton, N., P. Betzer, and P. Bull, 2001: Long-range transport of giantaeolian quartz grains: Linkage with discrete sedimentary sources and implications for protective particle transfer. *Mar. Geol.*, **177**, 411–417, https://doi.org/10.1016/S0025-3227(01)00171-2.

Modini, R. L., and Coauthors, 2015: Primary marine aerosol-cloud interactions off the coast of California. *J. Geophys. Res. Atmos.*, **120**, 4282–4303, https://doi.org/10.1002/2014JD022963.

Murphy, D. M., and Coauthors, 2019: The distribution of sea-salt aerosol in the global troposphere. *Atmos. Chem. Phys.*, **19**, 4093–4104, https://doi.org/10.5194/acp-19-4093-2019.

O'Dowd, C. D., J. A. Lowe, and M. H. Smith, 1999: Coupling sea-salt and sulphate interactions and its impact on cloud droplet concentration predictions. *Geophys. Res. Lett.*, **26**, 1311–1314, https://doi.org/10.1029/1999GL900231.

Pierce, J. R., and P. J. Adams, 2006: Global evaluation of CCN formation by direct emission of sea salt and growth of ultrafine sea salt. *J. Geophys. Res.*, **111**, D06203, https://doi.org/10.1029/2005JD006186.

Planes, S., and Coauthors, 2019: The Tara Pacific expedition—A pan-ecosystemic approach of the "-omics" complexity of coral reef holobionts across the Pacific Ocean. *PLOS Biol.*, **17**, e3000483, https://doi.org/10.1371/journal.pbio.3000483.

Prather, K. A., and Coauthors, 2013: Bringing the ocean into the laboratory to probe the chemical complexity of sea spray aerosol. *Proc Natl Acad Sci U S A*, **110**, 7550–7555, https://doi.org/10.1073/pnas.1300262110.

Quinn, P. K., D. B. Collins, V. H. Grassian, K. A. Prather, and T. S. Bates, 2015: Chemistry and related properties of freshly emitted sea spray aerosol. *Chem. Rev.*, **115**, 4383–4399, https://doi.org/10.1021/cr500713g.

——, D. J. Coffman, J. E. Johnson, L. M. Upchurch, and T. S. Bates, 2017: Small fraction of marine cloud condensation nuclei made up of sea spray aerosol. *Nat. Geosci.*, **10**, 674–679, https://doi.org/10.1038/ngeo3003.

Ramachandran, S., 2018: Aerosols and climate change: Present understanding, challenges, and future outlook. *Land-Atmospheric Research Applications in South and Southeast Asia*, K. P. Vadrevu, T. Ohara, and C. Justice, Eds., Springer International Publishing, 341–378.

Rinaldi, M., and Coauthors, 2010: Primary and secondary organic marine aerosol and oceanic biological activity: Recent results and new perspectives for future studies. *Adv. Meteor.*, **2010**, 1–10, https://doi.org/10.1155/2010/310682.

Rolph, G., A. Stein, and B. Stunder, 2017: Real-Time Environmental Applications and Display System: READY. *Environ. Modell. Software*, **95**, 210–228, https://doi.org/10.1016/j.envsoft.2017.06.025.

Smirnov, A., and Coauthors, 2006: Ship-based aerosol optical depth measurements in the Atlantic Ocean: Comparison with satellite retrievals and GOCART model. *Geophys. Res. Lett.*, **33**, L14817, https://doi.org/10.1029/2006GL026051.

Stein, A. F., R. R. Draxler, G. D. Rolph, B. J. B. Stunder, M. D. Cohen, and F. Ngan, 2015: NOAA's HYSPLIT atmospheric transport and dispersion modeling system. *Bull. Amer. Meteor. Soc.*, **96**, 2059–2077, https://doi.org/10.1175/BAMS-D-14-00110.1.

Textor, C., and Coauthors, 2006: Analysis and quantification of the diversities of aerosol life cycles within AeroCom. *Atmos. Chem. Phys.*, **6**, 1777–1813, https://doi.org/10.5194/acp-6-1777-2006.

Van der Does, M., P. Knippertz, P. Zschenderlein, R. Giles Harrison, and J.-B. W. Stuut, 2018: The mysterious long-range transport of giant mineral dust particles. *Sci. Adv.*, **4**, eaau2768, https://doi.org/10.1126/sciadv.aau2768.

Von der Weiden, S.-L., F. Drewnick, and S. Borrmann, 2009: Particle loss calculator–A new software tool for the assessment of the performance of aerosol inlet systems. *Atmos. Meas. Tech.*, **2**, 479–494, https://doi.org/10.5194/amt-2-479-2009.

Woodward, S., D. L. Roberts, and R. A. Betts, 2005: A simulation of the effect of climate change-induced desertification on mineral dust aerosol. *Geophys. Res. Lett.*, **32**, L18810, https://doi.org/10.1029/2005GL023482.

Wu, J., 1981: Evidence of sea spray produced by bursting bubbles. *Science*, **212**, 324–326, https://doi.org/10.1126/science.212.4492.324.